


**Unconventional properties of the noncentrosymmetric superconductor  $\text{Re}_8\text{NbTa}$** R. K. Kushwaha<sup>1</sup>, Arushi<sup>1</sup>, S. Sharma<sup>2</sup>, S. Srivastava<sup>1</sup>, P. K. Meena<sup>1</sup>, M. Pula<sup>2</sup>, J. Beare<sup>2</sup>, J. Gautreau<sup>2</sup>, A. D. Hillier<sup>3</sup>, G. M. Luke<sup>2,4</sup> and R. P. Singh<sup>1,\*</sup><sup>1</sup>*Department of Physics, Indian Institute of Science Education and Research Bhopal, Bhopal, 462066, India*<sup>2</sup>*Department of Physics and Astronomy, McMaster University, Hamilton, Ontario L8S 4M1, Canada*<sup>3</sup>*ISIS Facility, STFC Rutherford Appleton Laboratory, Didcot OX11 0QX, United Kingdom*<sup>4</sup>*TRIUMF, Vancouver, British Columbia V6T 2A3, Canada* (Received 15 January 2024; revised 18 April 2024; accepted 25 April 2024; published 13 May 2024)

Re-based superconductors provide a rich platform for the study of unconventional superconductivity. We have investigated the superconducting properties of  $\text{Re}_8\text{NbTa}$ , a new noncentrosymmetric cubic ( $\alpha$ -Mn structure) rhenium-based ternary superconductor using transport, magnetization, specific-heat, and muon-spin rotation/relaxation ( $\mu\text{SR}$ ) measurements. Specific-heat and transverse field  $\mu\text{SR}$  measurements suggest moderately coupled fully gapped superconductivity, well described by BCS theory. However, our zero-field  $\mu\text{SR}$  measurements reveal a small internal field onset around the superconducting  $T_c$ , indicating the unconventional superconducting ground state.

DOI: [10.1103/PhysRevB.109.174518](https://doi.org/10.1103/PhysRevB.109.174518)**I. INTRODUCTION**

An important question in the study of unconventional superconductivity is the role of fundamental symmetries such as time reversal and inversion in the pairing interaction and the resulting superconducting state [1,2]. The discovery of the noncentrosymmetric (NCS) superconductor  $\text{CePt}_3\text{Si}$  [1] attracted significant attention due to the absence of an inversion center in its crystal structure. This lack of inversion symmetry disrupts the degeneracy of electrons on the Fermi surface through antisymmetric spin-orbit coupling (ASOC) [3], resulting in the intriguing phenomenon of parity mixing [2,4]. These parity-mixed Cooper pairs have unveiled a plethora of captivating phenomena in NCS superconductors, such as a high upper critical field surpassing the Pauli limiting field [5,6], the emergence of a helical superconducting phase in the presence of a magnetic field (referred to as the FFLO state) [7,8], the presence of nodes or multigap behavior [9–12], the existence of topological superconducting phases [13], and the recent revelation of superconducting torofluxes, reminiscent of the Chandrasekhar-Kendall state [14]. In addition to these unconventional properties, some NCS superconductors have been reported to show spontaneous breaking of the time-reversal symmetry (TRS) within the superconducting state [4].

In recent years, extensive research has been focused on NCS superconductors [15–34], with a particular focus on rhenium-based NCS superconductors due to the frequent occurrence of TRS breaking [24–26,29]. However, despite crystallization in the NCS structure, some of these rhenium-based superconductors exhibit preserved TRS [21–23,27,28], while centrosymmetric rhenium-based superconductors and elemental rhenium break TRS [29] questioning the role of crystal structure in TRS breaking. Furthermore, a study focused

on the  $\text{Re}_{1-x}\text{Mo}_x$  series [35] compounds crystallized in centro/noncentrosymmetric crystal structure introduced the intriguing hypothesis that the ratio of rhenium to the transition metal (X) and the optimal percentage of rhenium could be factors that contribute to TRS breaking [36]. These observations have prompted inquiries into the potential roles of ASOC, its strength [24,37,38], and crystal structure in the context of TRS breaking in rhenium-based superconductors. Further research and microscopic measurements on new rhenium-based superconductors are necessary to fully understand the exact pairing mechanism. The ternary Re-based alloy,  $\text{Re}_8\text{NbTa}$ , offers an excellent opportunity for this purpose due to its mixed  $4d/5d$  site. This study also probes the role of disorder in time-reversal symmetry breaking (TRSB) in rhenium-based systems, an aspect which remains largely unexplored. Compared to the binary analog,  $\text{Re}_8\text{NbTa}$  introduces additional disorder due to the slight variation in the atomic size of Ta and Nb. This difference is evident in the lower residual resistivity ratio of  $\text{Re}_8\text{NbTa}$  compared to binary Re-based alloys [28,30].

In this paper, we provide the first microscopic investigation of the rhenium-rich ternary superconductor  $\text{Re}_8\text{NbTa}$ , characterized using AC transport, magnetization, specific-heat, and zero/transverse field muon-spin relaxation/rotation ( $\mu\text{SR}$ ) [39] measurements. Our transverse field  $\mu\text{SR}$  measurements indicate a fully gapped isotropic superconducting state, consistent with an s-wave pairing state [40]. Intriguingly, our zero field  $\mu\text{SR}$  results reveal TRSB in the superconducting state, indicating an unconventional nature to superconductivity in  $\text{Re}_8\text{NbTa}$ .

**II. EXPERIMENTAL DETAILS**

The polycrystalline  $\text{Re}_8\text{NbTa}$  sample was synthesized by melting high-purity metals (3N) Re, Nb, and Ta in a stoichiometric ratio under high-purity argon gas in an arc furnace followed by annealing at 1100°C for a week to remove

\*rpsingh@iiserb.ac.in

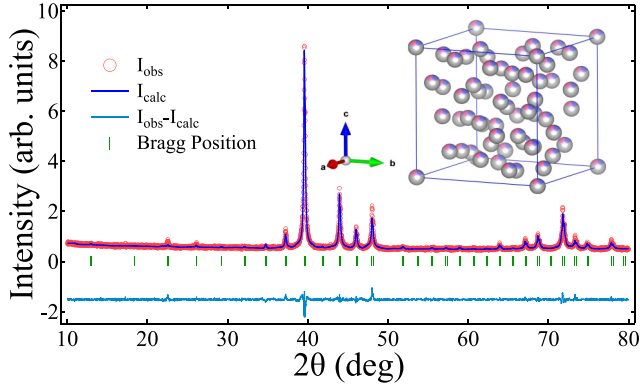


FIG. 1. The powder XRD pattern of  $\text{Re}_8\text{NbTa}$  is shown by pink circles, while the solid blue line represents the Rietveld refinement pattern. The inset shows the crystal structure of  $\text{Re}_8\text{NbTa}$ .

thermal strain from the sample. A PANalytical powder x-ray diffractometer equipped with  $\text{Cu-K}\alpha$  radiation ( $\lambda = 1.5406 \text{ \AA}$ ) was used to determine the crystal structure and phase purity. Magnetization was measured with a Quantum Design MPMS 3, while resistivity and specific heat were measured using a Quantum Design PPMS. Muon-spin rotation/relaxation experiments were conducted in transverse-field (TF) and zero-field (ZF) configurations to investigate the superconducting gap structure and identify any spontaneous field in the superconducting state, using the M20 beamline at the TRIUMF Center for Molecular and Material Science, in Vancouver, Canada. For the  $\mu\text{SR}$  measurements, the  $\text{Re}_8\text{NbTa}$  sample was cut into flat plates and held in the sample holder within the  $^4\text{He}$  gas flow cryostat using thin metalized Mylar tape, which is sufficiently thin to not stop any muons. Muons missing the sample landed in a veto detector, allowing us to collect background-free spectra. In the TF configuration, the initial orientation of the muon spins was prepared to be perpendicular to the magnetic field, which was applied parallel to the incoming muon beam momentum. A combination of a fluxgate magnetometer, muMetal, and three sets of perpendicular electromagnets was used to establish a zero magnetic field at the sample position [41]. Our  $\mu\text{SR}$  data were analyzed using the MUSRFIT software package [42].

### III. RESULTS AND DISCUSSION

#### A. Crystal structure characterization

The room-temperature powder x-ray diffraction (XRD) pattern of  $\text{Re}_8\text{NbTa}$  is shown in Fig. 1. Rietveld refinement using Fullprof software [43] confirms the phase purity and crystal structure as  $\alpha\text{-Mn}$  cubic with space group  $I43m$ . The lattice parameters and cell volume obtained from the refinement are as follows:  $a = b = c = 9.654(9) \text{ \AA}$  and  $V_{\text{cell}} = 899.8(9) \text{ \AA}^3$ .

#### B. Electrical resistivity

Figure 2(a) shows the temperature-dependent resistivity [ $\rho(T)$ ] of  $\text{Re}_8\text{NbTa}$ , measured from 1.9 to 300 K in zero magnetic field. Figure 2(b) shows a distinct decrease in resistivity at critical temperature  $T_c^{\text{drop}} = 8.1(1) \text{ K}$ , with a

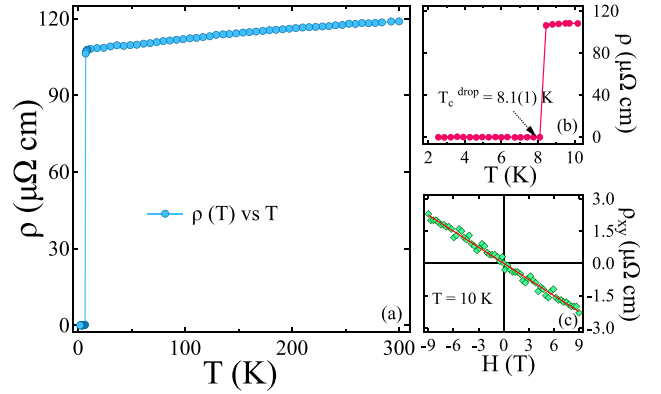


FIG. 2. (a) Temperature dependence of zero-field resistivity,  $\rho(T)$  (b) A sharp zero drop in resistivity at  $T_c^{\text{drop}} = 8.1(1) \text{ K}$ . (c) Hall resistivity ( $\rho_{xy}$ ) at 10 K under a magnetic field of  $\pm 9 \text{ T}$ .

transition width of 0.5 K, which, along with magnetization and specific-heat measurements discussed later, confirms bulk superconductivity in  $\text{Re}_8\text{NbTa}$ . The residual resistivity ratio  $[\text{RRR} = \rho(300 \text{ K})/\rho(10 \text{ K})] = 1.1$  implies a highly disordered nature and is in agreement with other Re-based alloys crystallizing in the  $\alpha\text{-Mn}$  structure [24–26,28].

#### C. Magnetization

Magnetization measurements were performed in zero field-cooled warming (ZFCW) and field-cooled cooling (FCC) in an applied magnetic field of 1 mT. It confirms the superconducting transition temperature of  $\text{Re}_8\text{NbTa}$  at 7.7(4) K by exhibiting a strong diamagnetic signal as shown in Fig. 3(a) and the inset shows the full range  $M(H)$  curve from  $-7 \text{ T}$  to  $7 \text{ T}$ . This magnetization loop defines the irreversibility field  $H_{\text{irr}} = 3.1(2) \text{ T}$ , above which the unpinning of the vortices takes place. The lower critical field,  $H_{c1}(0)$ , was determined from the low-field magnetization curves taken at different temperatures from 1.8 to 7.5 K, which are shown in the inset of Fig. 3(b). The lower critical field corresponding to every temperature curve was considered as the point that deviates from the linearity relation [shown by the solid black line in the inset of Fig. 3(b)].  $H_{c1}(0)$  was found to be 6.49(4) mT from the fit utilizing the Ginzburg-Landau (GL) relation

$$H_{c1}(T) = H_{c1}(0) \left[ 1 - \left( \frac{T}{T_c} \right)^2 \right]. \quad (1)$$

The upper critical field  $H_{c2}(0)$  was estimated by measuring the effect of the applied field on the transition temperature using different techniques: magnetization [ $M(T, H)$ ], specific heat [ $C(T, H)$ ], and resistivity [ $\rho(T, H)$ ]. Figure 4(c) shows  $C(T, H)$  where  $T_c$  is suppressed only down to 3.54 K in the presence of a field of 9 T, suggesting a high value of the upper critical field. In  $M(T, H)$ , the onset of the diamagnetic signal is considered as  $T_c$ , while the midpoint of the jump and the drop in  $C(T, H)$  and  $\rho(T, H)$  [see the inset of Fig. 3(c)], respectively, are taken as criteria for  $T_c$ .  $H_{c2}(T)$  of all measurements was plotted against the reduced temperature ( $T/T_c$ ), and a linear response was observed near  $T/T_c = 1$ , which can be well described by the GL relation for the upper

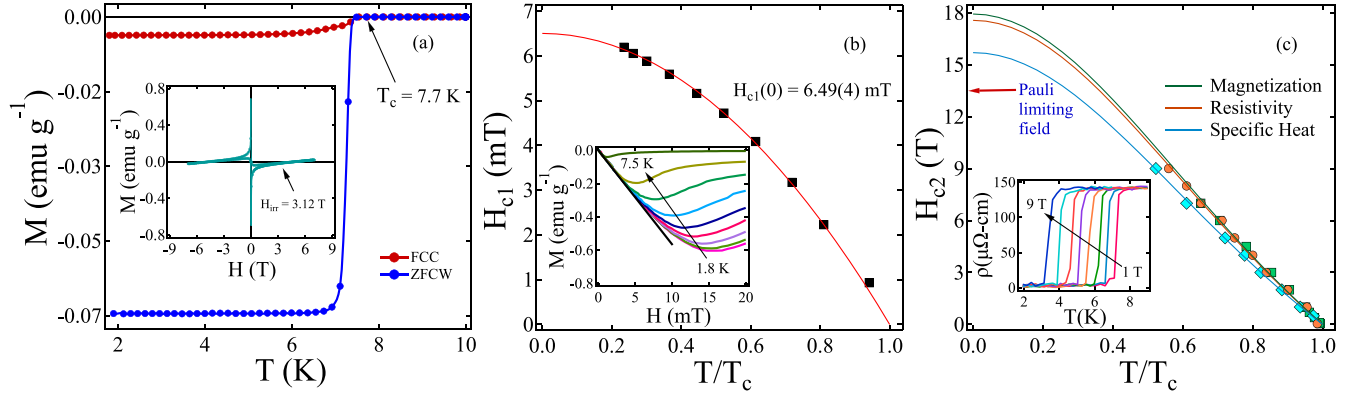


FIG. 3. (a) The temperature dependence of the moment in the ZFCW and FCC mode under an applied magnetic field of 1 mT. The inset shows the  $M(H)$  loop at 1.8 K under an applied field of  $\pm 7$  T. (b) Lower critical field vs reduced temperature ( $T/T_c$ ). The inset provides  $M(H)$  curves at various temperatures. (c) The upper critical field vs the reduced temperature ( $T/T_c$ ), estimated from magnetization, resistivity, and specific-heat measurements. Solid lines represent the Ginzburg-Landau (GL) fit using equation Eq. (2), with the inset showing the variation of resistivity with temperature in various magnetic fields.

critical field which follows

$$H_{c2}(T) = H_{c2}(0) \left[ \frac{1-t^2}{1+t^2} \right], \quad (2)$$

where  $t = T/T_c$  and the fit using Eq. (2) yields  $H_{c2}(0) = 17.9(2)$  T,  $17.5(3)$  T, and  $15.7(4)$  T from magnetization, resistivity, and specific-heat measurements, respectively. Such high values of  $H_{c2}(0)$  were also found for other NCS rhenium-based alloys [24,28], which indicates the possibility of a strong ASOC and unconventional characteristic in the superconducting state of  $\text{Re}_8\text{NbTa}$  [1,2].

Two independent Cooper pair-breaking processes can be considered with an external magnetic field application: the orbital pair-breaking effect and the Pauli limiting field effect. Orbital pair breaking occurs when the kinetic energy of one electron is increased so that the Lorentz force breaks the Cooper pair and the field at which the Cooper pair is broken, termed the orbital limiting field, which the Werthamer-Helfand-Hohenberg model provides [44,45]

$$H_{c2}^{\text{orb}}(0) = -\alpha T_c \left. \frac{dH_{c2}(T)}{dT} \right|_{T=T_c}, \quad (3)$$

At  $T = T_c$ , the initial slope  $\frac{-dH_{c2}(T)}{dT}$  for  $\text{Re}_8\text{NbTa}$  was found to be  $3.16(7)$  T/K and by taking  $\alpha = 0.693$  (for dirty limit superconductors), orbital limiting upper critical field,  $H_{c2}^{\text{orb}}(0) = 15.5(1)$  T. In the realm of BCS superconductors, the Pauli limiting field is given by  $H_{c2}^p = C \times T_c$ , where  $C = 1.86$  T/K [5,6], and for  $\text{Re}_8\text{NbTa}$  with  $T_c = 7.7(4)$  K,  $H_{c2}^p = 14.3(2)$  T. Both pair-breaking limiting upper critical fields are less than the estimated  $H_{c2}(0)$  values obtained from three different measurements mentioned above, suggesting a possible unconventional superconducting nature in  $\text{Re}_8\text{NbTa}$ .

Two fundamental length scales of a superconductor, coherence length and penetration depth, can be computed using the values of  $H_{c1}(0)$  and  $H_{c2}(0)$ . In GL theory, the coherence length  $\xi_{\text{GL}}(0)$  [46] and the penetration depth  $\lambda_{\text{GL}}(0)$  [47] were defined according to the relations  $H_{c2}(0) = \frac{\Phi_0}{2\pi\xi_{\text{GL}}^2}$  and  $H_{c1}(0) = \frac{\Phi_0}{4\pi\lambda_{\text{GL}}^2} [\ln \frac{\lambda_{\text{GL}}(0)}{\xi_{\text{GL}}(0)} + 0.12]$ , respectively, where  $\Phi_0 (= 2.07 \times 10^{-15}$  T m<sup>2</sup>) is the magnetic flux quantum [46]. Using  $H_{c1}(0) = 6.49(4)$  mT and  $H_{c2}(0) = 17.9(1)$  T,  $\xi_{\text{GL}}(0)$  and  $\lambda_{\text{GL}}(0)$  were evaluated to be  $42.8(7)$  Å and  $3371(2)$  Å, respectively. The GL parameter defined

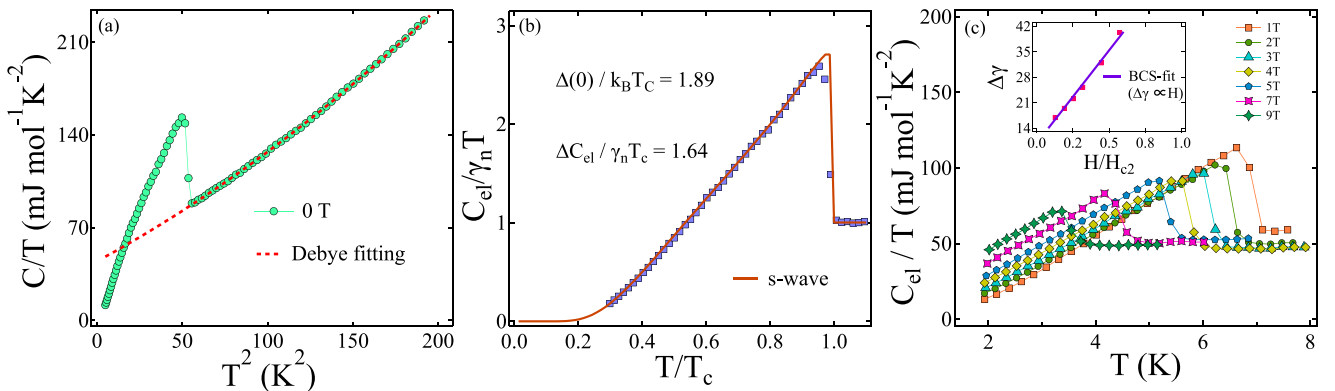


FIG. 4. (a) Zero-field  $C/T$  variation to  $T^2$  with the red dotted line representing the fit to Eq. (5). (b) Normalized electronic-specific heat is best described by the isotropic single-gap model (solid orange line). (c)  $C_{el}/T$  vs  $T$  in various magnetic fields; the inset indicates a BCS-type single-gap structure, as the field-dependent residual electronic specific-heat coefficients are shown following a straight line.

as  $k_{GL} = \frac{\lambda_{GL}(0)}{\xi_{GL}(0)} = 78.6(2)$ , indicating  $\text{Re}_8\text{NbTa}$  is a strong type II superconductor.

The Ginzburg-Levanyuk number  $Gi$  represents the strength of the thermal fluctuations over the vortex unpinning in the superconducting state and is given by Eq. (4),

$$Gi = \frac{1}{2} \left[ \frac{k_B \mu_0 \tau T_c}{4\pi \xi(0)^3 H_c^2(0)} \right]^2, \quad (4)$$

where the anisotropy factor  $\tau$  is 1 for cubic  $\text{Re}_8\text{NbTa}$ . Using  $T_c = 7.7(4)$  K,  $\xi(0) = 42.8(7)$  Å, and  $H_c(0) = 163.3(6)$  mT, we obtained  $Gi = 12.2(1) \times 10^{-6}$  which is greater than the typical values of low- $T_c$  superconductors ( $10^{-8}$ ) [48] but less than the value of high- $T_c$  cuprate superconductors ( $10^{-2}$ ) [49], suggesting that weak thermal fluctuations are responsible for the unpinning of vortices [50] in  $\text{Re}_8\text{NbTa}$ .

#### D. Specific heat

Figure 4(b) shows the variation of normalized electronic specific heat with reduced temperature ( $T/T_c$ ) in zero field. A sharp jump at the  $T_{c,\text{mid}} = 7.5(1)$  K is aligning with the drop in resistivity and the onset of diamagnetism, confirms the bulk superconductivity in  $\text{Re}_8\text{NbTa}$ . In general, the normal state low-temperature specific-heat data can be described by the Debye-Sommerfeld model,

$$C/T = \gamma_n + \beta_3 T^2 + \beta_5 T^4, \quad (5)$$

where  $\gamma_n$  represents the Sommerfeld coefficient providing electronic contributions to the specific heat and  $\beta_3$  and  $\beta_5$  represent the phononic and anharmonic contributions to the specific heat, respectively. A fit to the specific-heat data using Eq. (5) as shown in Fig. 4(a), yields  $\gamma_n = 44.5(4)$  mJ mol<sup>-1</sup> K<sup>-2</sup>, which is relatively high as found in other intermetallic compounds like  $\text{La}_7\text{X}_3$  ( $X = \text{Ni}, \text{Ir}$ ) (44.43 mJ mol<sup>-1</sup> K<sup>-2</sup> in  $\text{La}_7\text{Ni}_3$  [33] and 47 mJ mol<sup>-1</sup> K<sup>-2</sup> in  $\text{La}_7\text{Ir}_3$  [31]) due to moderate electronic correlation,  $\beta_3 = 0.695(6)$  mJ mol<sup>-1</sup> K<sup>-4</sup>, and  $\beta_5 = 1.30(2)$  μJ mol<sup>-1</sup> K<sup>-6</sup>.  $\gamma_n$  is related to the density of states at Fermi level  $D_c(E_F)$  by the relation  $\gamma_n = (\frac{\pi^2 k_B^2}{3}) D_c(E_F)$ , where  $k_B \simeq 1.38 \times 10^{-23}$  J K<sup>-1</sup>.  $D_c(E_F)$  is estimated to be 18.9(1) states/eV f.u. for  $\text{Re}_8\text{NbTa}$ . According to the Debye model, the Debye temperature ( $\theta_D$ ) can be obtained from  $\beta_3$  using the formula  $\theta_D = (\frac{12\pi^4 RN}{5\beta_3})^{1/3}$ , where  $N$  is the number of atoms per formula unit and  $R$  is the molar gas constant (8.314 J mol<sup>-1</sup> K<sup>-1</sup>), giving  $\theta_D = 303(1)$  K.

The electron-phonon coupling strength estimated using McMillan's model [51]

$$\lambda_{e\text{-ph}} = \frac{1.04 + \mu^* \ln(\theta_D/1.45T_c)}{(1 - 0.62\mu^*) \ln(\theta_D/1.45T_c) - 1.04}, \quad (6)$$

where  $\mu^*$  represents screened Coulomb repulsion, considering  $\mu^* = 0.13$  as mentioned for all transition metals [51],  $\theta_D = 303(1)$  K and  $T_c = 7.5(1)$  K. We have obtained  $\lambda_{e\text{-ph}} = 0.73$ , classifying  $\text{Re}_8\text{NbTa}$  as a moderately coupled superconductor. The electronic contribution to the specific heat can be calculated after subtracting the phononic contribution ( $C_{\text{ph}}$ ) from the total specific heat as  $C_{\text{el}} = C - C_{\text{ph}} = C - \beta_3 T^3 - \beta_5 T^5$ . The normalized electronic specific-heat jump  $\Delta C_{\text{el}}/\gamma_n T_c = 1.64$ , higher than the standard value of 1.43 for

BCS superconductors in the weak-coupling limit, suggests moderate electron-phonon coupling in  $\text{Re}_8\text{NbTa}$  [52,53].

We have also performed field-dependent specific-heat measurements to investigate the gap structure via the residual electronic specific-heat coefficient in the magnetic field [ $\Delta\gamma = \gamma(H) - \gamma(0)$ ] in a conventional superconductor ( $\Delta\gamma$ )  $\propto H$  for a nodeless gap [54]. The electronic specific-heat coefficient was calculated by fitting the  $C_{\text{el}}/T$  vs  $T$  curves [as shown in Fig. 4(c)] at different magnetic fields using the following relation [55]:

$$\frac{C_{\text{el}}}{T} = \gamma + \left(\frac{a}{T}\right) \exp\left(-b\frac{T_c}{T}\right). \quad (7)$$

The inset of Fig. 4(c) represents the linear dependence of  $\Delta\gamma$  relative to the reduced magnetic field ( $H/H_{c2}$ ) confirming the fully gapped superconductivity [54,56].

The absence of noticeable temperature dependence in the electronic specific heat at low temperatures typically indicates a single, nodeless gap. Analyzing the temperature-dependent electronic specific heat allows us to explore the symmetry of the superconducting gap. Normalized entropy ( $S$ ) in the superconducting region and electronic-specific heat can be related as  $C_{\text{el}} = t \frac{dS}{dt}$ , where  $t = T/T_c$  is the reduced temperature. Within the BCS approximation, the normalized entropy for a single gap is defined by the following relation:

$$\frac{S}{\gamma_n T_c} = -\frac{6}{\pi^2} \left[ \frac{\Delta(0)}{k_B T_c} \right] \int_0^\infty [f \ln(f) + (1-f) \ln(1-f)] dy, \quad (8)$$

where  $f(\xi) = [\exp(E(\xi)/k_B T) + 1]^{-1}$  is the Fermi distribution,  $E(\xi) = \sqrt{\xi^2 + \Delta^2(t)}$ ,  $E(\xi)$  is the energy of the normal electrons measured relative to the Fermi energy,  $y = \xi/\Delta(0)$ , and  $\Delta(t) = \tanh(1.82\{1.018[(1/t) - 1]\}^{0.51})$  is the BCS approximation for temperature-dependent superconducting energy gap. The solid orange line in Fig. 4(b) represents the fit to the electronic specific-heat data with the single isotropic BCS gap model. We obtain a normalized gap value,  $\Delta(0)/k_B T_c = 1.89$ , slightly higher than the weakly coupled BCS value (1.76). This increase in both  $\Delta C_{\text{el}}/\gamma_n T_c$  and  $\Delta(0)/k_B T_c$  values compared to BCS values has also been observed for other Re-based binary alloys crystallizing in the  $\alpha$ -Mn structure [25,26,28,35], indicating a moderate electron-phonon coupling in those materials and here for  $\text{Re}_8\text{NbTa}$ . Further, the thermodynamic critical field ( $H_c$ ) was estimated using  $\alpha$ -model equation  $H_c(0) = \alpha T_c (\frac{6\gamma_{nv}}{\pi})^{1/2}$ , where  $\gamma_{nv}$  is the Sommerfeld coefficient per unit volume. For  $\text{Re}_8\text{NbTa}$ ,  $\gamma_{nv} = 4454(40)$  erg cm<sup>-1</sup> K<sup>-2</sup> and  $\alpha = \Delta(0)/k_B T_c = 1.89$ , which yields  $H_c(0) = 130.7(4)$  mT.

#### E. Muon spin rotation/relaxation

##### 1. Transverse-field $\mu\text{SR}$

To investigate the superconducting gap symmetry, we performed muon-spin rotation and relaxation measurements in the TF configuration. To generate a well-ordered flux line lattice (FLL), the field-cooled method was employed where a magnetic field  $H_{c1} < H \ll H_{c2}$  was first applied in the normal state, and then the sample was cooled to low temperature. The asymmetry spectra recorded below

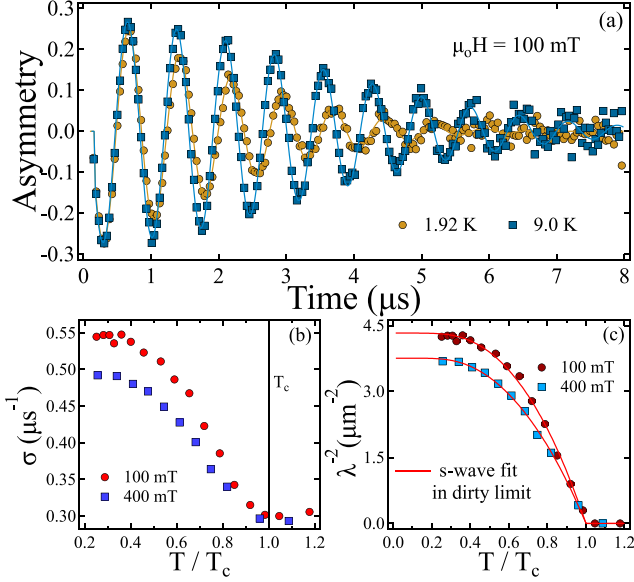


FIG. 5. (a) TF- $\mu$ SR asymmetry spectra recorded from 1.8 to 10.0 K at 100 mT. Plots at 1.92 K and 9 K in a rotating reference frame of 90 mT highlight changes upon flux-line lattice formation in the superconducting state. Solid lines depict fits using Eq. (9). (b) TF- $\mu$ SR depolarization rate  $\sigma$  at 100 mT and 400 mT vs reduced temperature  $T/T_c(H)$  (c) Inverse squared penetration depth vs reduced temperature  $T/T_c(H)$  in 100 and 400 mT for  $\text{Re}_8\text{NbTa}$ .

and above  $T_c$  are presented in Fig. 5(a). The difference in the depolarization rate for the  $T < T_c$  spectra compared to the above  $T_c$  can be explained by the presence of an inhomogeneous field distribution due to FLL formation. The weak Gaussian damping for the  $T > T_c$  spectra corresponds to the relaxation of randomly oriented nuclear dipole fields. The time-domain spectra are well described using the oscillatory function multiplied with Gaussian relaxation,

$$A_{\text{TF}}(t) = A \exp\left(\frac{-\sigma^2 t^2}{2}\right) \cos(\omega t + \phi), \quad (9)$$

where  $A$  is the asymmetry,  $\sigma$  is the relaxation rate of the sample,  $\phi$  is the initial phase, and  $\omega$  is the precession frequency. The total depolarization of the sample  $\sigma$  includes the contribution of FLL in the superconducting state  $\sigma_{\text{sc}}$  and a small contribution from randomly oriented nuclear dipole moments  $\sigma_{\text{nm}}$ . Figure 5(b) shows the fit values of  $\sigma$  as a function of the reduced temperature ( $T/T_c$ ) for  $\text{Re}_8\text{NbTa}$  obtained in the applied field of 100 and 400 mT. Due to the formation of FLL in the superconducting state, the field distribution becomes inhomogeneous, resulting in an increase in  $\sigma$  below  $T_c$ . The temperature-independent nuclear contribution to the depolarization rates is taken to be  $\sigma_{\text{nm}} = 0.2999(2)$  and  $0.2934(1) \mu\text{s}^{-1}$  at 100 and 400 mT, respectively, equal to the average depolarization rate,  $\sigma$ , above  $T_c$ .

The total depolarization rate is given by

$$\sigma^2 = \sigma_{\text{sc}}^2 + \sigma_{\text{nm}}^2. \quad (10)$$

Using Eq. (10) and the measured normal state relaxation rate, we extracted the superconducting contribution to the relaxation rate  $\sigma_{\text{sc}}$ .  $\sigma_{\text{sc}}$  is related to the mean-square inhomogeneity in the field [57],  $\langle(\Delta B)^2\rangle$  as

$$\sigma_{\text{sc}}^2 = \gamma_\mu^2 \langle(\Delta B)^2\rangle, \quad (11)$$

where  $\gamma_\mu = 2\pi \times 135.5 \text{ MHz/T}$  is the muon gyromagnetic ratio.

For a triangular Abrikosov vortex lattice, the penetration depth can be calculated from the relaxation rate of FLL using Brandt's formula [58],

$$\sigma_{\text{sc}}(T) = \frac{0.0609 \times \gamma_\mu \phi_0}{[\lambda^\mu(T)]^2}, \quad (12)$$

Here  $\phi_0$  is the magnetic flux quantum.

The reduced temperature variation of  $(\lambda^\mu)^{-2}$  is shown in Fig. 5(c). We have used the fitting function for the temperature dependence of  $(\lambda^\mu)^{-2}$  using London's approximation for a BCS superconductor in the dirty limit [59],

$$\frac{\sigma_{\text{sc}}(T)}{\sigma_{\text{sc}}(0)} = \frac{[\lambda^\mu(T)]^{-2}}{[\lambda^\mu(0)]^{-2}} = \frac{\Delta(T)}{\Delta(0)} \tanh\left[\frac{\Delta(T)}{2k_B T}\right], \quad (13)$$

where  $\Delta(T) = \Delta(0) \tanh(1.82\{1.018[(T_c/T) - 1]\}^{0.51})$ , the temperature dependence of the energy gap in the BCS approximation, and  $\Delta(0)$  is the energy gap value at 0 K. Our results for this fitting, illustrated in Fig. 5(c), give  $\Delta(0)$  values of 1.20(1) and 1.09(1) meV at 100 and 400 mT, respectively. We also obtain  $\sigma_{\text{sc}}(0) = 0.4497(9)$  and  $0.3949(5) \mu\text{s}^{-1}$  and the corresponding magnetic penetration depth at 0 K is estimated as  $\lambda^\mu(0) = 458(1)$  and  $521(2) \text{ nm}$  at 100 and 400 mT, respectively. Apart from the estimation of  $H_{c1}(0)$  from magnetization, we have calculated the  $H_{c1}(0)$  value from TF- $\mu$ SR measurement as discussed in Ref. [58], which provides  $H_{c1}(0) = 4.04(1) \text{ mT}$ . The excellent fit to Eq. (13) is consistent with fully gapped  $s$ -wave superconductivity, in agreement with our specific-heat results. The normalized superconducting gap value,  $\Delta(0)/k_B T_c = 1.88(2)$  at 100-mT field which further reduced to 1.72(2) at 400 mT, aligns closely with the value obtained from the specific heat (1.89), suggesting a moderate electron-phonon coupling in the superconducting state of  $\text{Re}_8\text{NbTa}$ .

## 2. Zero-field $\mu$ SR

Zero-field  $\mu$ SR measurements were carried out to detect possible TRSB in the superconducting state of  $\text{Re}_8\text{NbTa}$ . Relaxation spectra were collected in the absence of any magnetic field, and two of these spectra recorded below ( $T = 1.8 \text{ K}$ ) and above ( $T = 8.5 \text{ K}$ )  $T_c$  are shown in Fig. 6(a). There were no oscillatory components in the spectra, which indicates the absence of any magnetic ordering. In the SC state, a slight enhancement of the relaxation in the superconducting state shown in Fig. 6(a) points to the presence of increased internal magnetic fields below  $T_c$ . Asymmetry spectra can be modeled for static and randomly oriented nuclear moments using the Gaussian Kubo-Toyabe (KT) function [60],

$$G_{\text{KT}}(t) = \frac{1}{3} + \frac{2}{3}(1 - \Delta^2 t^2) e^{-\frac{\Delta^2 t^2}{2}}, \quad (14)$$

where  $\Delta$  resembles the relaxation rate due to the densely packed, randomly oriented nuclear dipoles. To fit our data, we used the following function, which is the product of  $G_{\text{KT}}(t)$

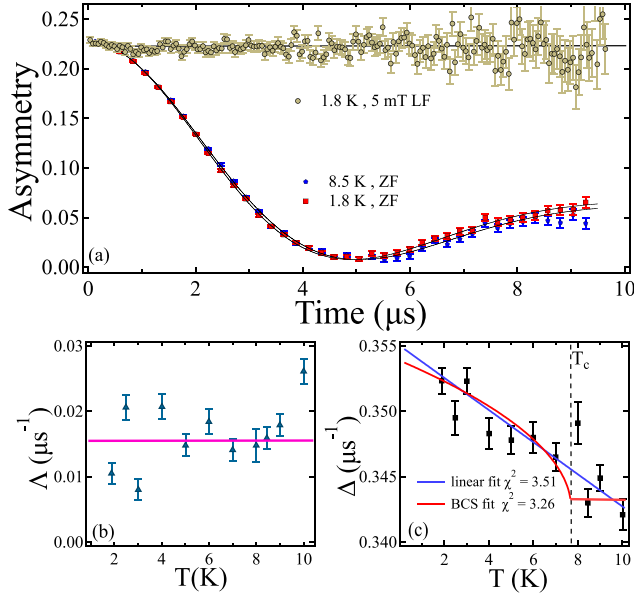


FIG. 6. (a) ZF- $\mu$ SR spectra collected below (1.8 K) and above (8.5 K)  $T_c$  and fitted using the Gaussian Kubo-Toyabe function as Eq. (15). (b) Temperature dependence of electronic relaxation rate  $\Delta$  with no noticeable change near  $T_c$ . (c) Temperature dependence of nuclear relaxation rate  $\Delta$  shows a notable increase below  $T_c$ .

with an exponential function:

$$A(t) = A_i G_{KT}(t)e^{-\Delta t}, \quad (15)$$

where  $A_i$  is the initial asymmetry and  $\Delta$  is the exponential relaxation rate. Figure 6(a) shows a small difference that indicates an additional relaxation of the muon-spin polarization below  $T_c$ . Our ZF- $\mu$ SR data are well fitted using Eq. (15). We found that the exponential term remained small and temperature independent through the superconducting transition as shown in Fig. 6(b), while an increase in the Kubo-Toyabe relaxation rate  $\Delta$  below  $T_c$  [see Fig. 6(c)] indicates the presence of a small spontaneous magnetic field in the superconducting state. We also performed longitudinal field- $\mu$ SR measurements to exclude the possibility of obtaining an increased relaxation from dilute fluctuating impurities. Applying a field of 5 mT parallel to the muon-spin direction at 1.8 K was sufficient to decouple the muon-spin polarization from the internal magnetic fields, as evidenced by the essentially flat spectrum in Fig. 6(a), indicating that the relaxation seen in ZF primarily corresponds to static internal fields. The magnitude of the internal magnetic field appearing below  $T_c$  can be estimated [26] from

$$B_{\text{int}} = \sqrt{2} \frac{\delta\Delta}{\gamma_\mu}, \quad (16)$$

where  $\delta\Delta$  is the increase in the Gaussian relaxation rate ( $\Delta$ ) in ZF mode below  $T_c$ ,  $0.0094(2) \mu\text{s}^{-1}$ , which corresponds to the internal field  $B_{\text{int}} = 0.15(1)$  G. This value of  $B_{\text{int}}$  for  $\text{Re}_8\text{NbTa}$  is comparable to the values found in previously reported NCS rhenium-based TRSB superconductors listed in Table I. We note that the same order of internal magnetic

TABLE I. Internal magnetic field obtained from ZF- $\mu$ SR measurement.

Compound	$B_{\text{int}}$ (Gauss)
$\text{Re}_8\text{NbTa}$	0.15
$\text{Re}_6\text{Ti}$	0.14
$\text{Re}_{24}\text{Ti}_5$	0.13
$\text{Re}_6\text{Zr}$	0.11
$\text{Re}_6\text{Hf}$	0.085

field corresponding to the change in the exponential relaxation rate was also found in  $\text{LaNiC}_2$  [61] and  $\text{La}_7\text{X}_3$  [31–33]. This observation indicates possible TRSB in  $\text{Re}_8\text{NbTa}$ , whereas the linear fit ( $\chi^2 = 3.51$ ) along with the BCS fit ( $\chi^2 = 3.26$ ) in  $\Delta(T)$  as represented in Fig. 6(c), points to the possibility of spin-fluctuation also, as discussed for  $\text{Re}_{5.5}\text{Ta}$  [28]. A similar linear trend in the relaxation rate was also observed in  $\text{Cs}_2\text{Cr}_3\text{As}_3$  [62] and  $(\text{Lu}, \text{Y})\text{RuB}_2$  [63] where the possible presence of spin fluctuation was proposed. These results suggest the unconventional superconducting ground state in  $\text{Re}_8\text{NbTa}$ .

### F. Electronic properties and the Uemura plot

To get a deeper understanding of the electronic properties of  $\text{Re}_8\text{NbTa}$ , we have utilized normal and superconducting state parameters derived from specific heat and Hall measurements using a simple Sommerfeld model assuming a 3D spherical Fermi surface. Hall resistivity ( $\rho_{xy}$ ) measured at 10 K in magnetic field  $\pm 9$  T, to estimate the quasiparticle number density [see Fig. 2(c)].  $\rho_{xy}(H)$  is fitted with a linear equation and the slope provides the Hall coefficient  $R_H = -2.06(1) \times 10^{-10} \Omega \cdot \text{m T}^{-1}$ . The negative slope indicates the electron-dominated charge carriers. The quasiparticle number density ( $n_e$ ) is related to the Hall coefficient by expression  $R_H = -1/e n_e$ , which yields  $n_e = 29.1(2) \times 10^{27} \text{m}^{-3}$ . This enables the estimation of the Fermi wave vector  $k_F = 0.95(1) \text{\AA}^{-1}$  using the equation  $k_F = (3\pi^2 n_e)^{1/3}$ . The effective mass was estimated as  $m^* = 11.28(7) m_e$  by the relation  $m^* = \frac{(\hbar k_F)^2 \gamma_n}{\pi^2 n_e k_B}$ . Following Drude's model for elec-

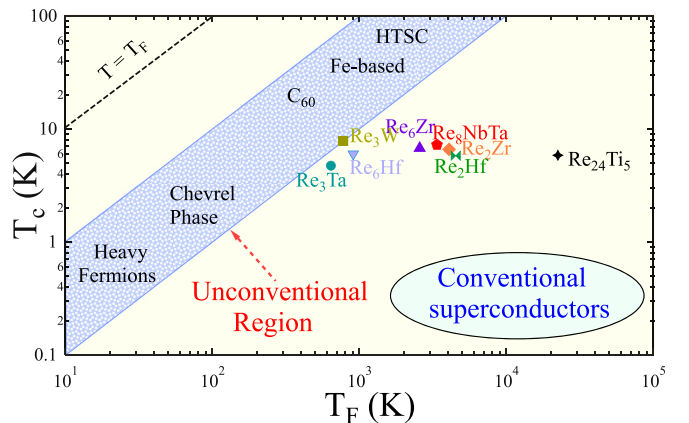


FIG. 7. Uemura plot between  $T_c$  and  $T_F$ ,  $\text{Re}_8\text{NbTa}$  is shown as a red pentagon which lies outside the unconventional band.

TABLE II. Superconducting and normal state parameters of  $\text{Re}_8\text{NbTa}$  with  $\text{Re}_{5.5}\text{Ta}$  [28] and  $\text{Re}_{0.82}\text{Nb}_{0.18}$  [29,30].

Parameters	$\text{Re}_8\text{NbTa}$	$\text{Re}_{5.5}\text{Ta}$	$\text{Re}_{0.82}\text{Nb}_{0.18}$
$T_c$ (K)	7.7(4)	8.0	8.8
$H_{c1}(0)$ (mT)	6.49(4)	3.23	5.56
$H_{c2}(0)$ (T)	17.9(2)	16.47	17.3
$H_{c2}(0)^P$ (T)	14.3(2)	14.78	16.8
$H_{c2}(0)^{\text{orb}}$ (T)	15.5(1)	9.33	14.04
$\Delta C_{\text{el}}/\gamma_n T_c$	1.64(2)	2.04	1.86
$\Delta(0)/k_B T_c$	1.89(1)	1.99	1.83
$\gamma_n$ ( $\text{mJ mol}^{-1}\text{K}^{-2}$ )	44.5(4)	25.3	53.5
$\theta_D$ (K)	303(1)	310	383.1
$\lambda_{e\text{-ph}}$	0.73(2)	0.73	0.73
$\xi_{\text{GL}}(0)$ ( $\text{\AA}$ )	42.8(7)	45	43.6
$\lambda_{\text{GL}}(0)$ ( $\text{\AA}$ )	3371(2)	4949	3625
$k_{\text{GL}}$	78.6(2)	111	83.14
$\lambda^\mu(0)$ (nm)	458(1)	422	357
$\lambda_{\text{GL}}^{\text{dirty}}(0)$ (nm)	418(2)	—	—
$v_F$ ( $10^5 \text{ ms}^{-1}$ )	0.98(2)	12.17	—
$n$ ( $10^{27} \text{ m}^{-3}$ )	29.1(2)	2.8	—
$T_F$ (K)	3376(90)	2040	—
$T_c/T_F$	0.002(1)	0.0038	—
$m^*/m_e$	11.28(7)	4.15	—

trical transport, the mean free path is defined as  $l_e = v_F \tau$ , where  $v_F = \frac{\hbar k_F}{m^*}$ , the Fermi velocity, and average scattering time  $\tau = \frac{m^*}{n_e e^2 \rho_0}$ , where residual resistivity  $\rho_0 = 108.6(3) \mu\Omega\text{-cm}$ . Using estimated values of  $m^*$ ,  $n_e$ , and  $\rho_0$ , we obtain  $\tau = 0.126(3) \times 10^{-13}$  s and  $v_F = 0.98(2) \times 10^5 \text{ m s}^{-1}$ . The mean free path is estimated to be  $l_e = 12.34(1) \text{\AA}$ . The BCS coherence length is defined as  $\xi_0 = \frac{0.18 \hbar v_F}{k_B T_c} = 186.4(7) \text{\AA}$ , higher than the GL coherence length obtained from  $H_{c2}(0)$ . Since  $\xi_0 \gg l_e$ ,  $\text{Re}_8\text{NbTa}$  is classified as a superconductor in a dirty limit. The GL penetration depth in dirty limit, at  $T = 0$  K is defined as  $\lambda_{\text{GL}}^{\text{dirty}}(0) = \lambda_L(1 + \frac{\xi_0}{l_e})^{1/2}$ , where  $\lambda_L = (\frac{m^*}{\mu_0 n_e e^2})^{1/2}$ , the London penetration depth in the dirty limit,

which evaluates  $\lambda_{\text{GL}}^{\text{dirty}}(0) = 418(2)$  nm. Notably, this value aligns closely with  $\lambda^\mu(0)$  obtained from our TF- $\mu$ SR measurement at 100 mT. Considering superfluid density  $n_s$  at  $T = 0$  K is equivalent to  $n_e$  above  $T_c$  [63], the Fermi temperature is defined as follows [63,64]:

$$k_B T_F = \left( \frac{\hbar^2}{2m^*} \right) (3\pi^2 n_s)^{2/3}. \quad (17)$$

Equation (17) yields  $T_F = 3376(90)$  K. The calculated ratio  $\frac{T_c}{T_F} = 0.002$  places  $\text{Re}_8\text{NbTa}$  in proximity to other rhenium-based superconductors [21–26,65] within the Uemera plot (see Fig. 7) [66]. All superconducting and normal state parameters of  $\text{Re}_8\text{NbTa}$  are listed in Table II.

#### IV. CONCLUSION

In conclusion, we have synthesized a new ternary non-centrosymmetric bulk superconductor  $\text{Re}_8\text{NbTa}$  having a  $T_c$  of 7.7(4) K with an upper critical field surpassing the Pauli limiting field. The superconducting gap  $\Delta(0)/k_B T_c = 1.89$ , and the electron-phonon coupling strength  $\lambda_{e\text{-ph}} = 0.73$ , point to a robust electron-phonon interaction suggesting moderately coupled superconductivity. Temperature-dependent electronic specific heat and TF- $\mu$ SR measurements confirm the existence of a nodeless superconducting gap. Additionally, ZF- $\mu$ SR results unveil an unconventional superconducting state, but almost-linear temperature dependence of  $\Delta$  suggests the possible presence of spin fluctuation and strong confirmation of TRSB needs further investigation with a wider temperature range.

#### ACKNOWLEDGMENTS

R.K.K. acknowledges the UGC Government of India for the Senior Research Fellowship (SRF). R.P.S. thanks Science and Engineering Board (SERB), Government of India, for the Core Research Grant No. CRG/2023/000817. Work at McMaster University received support from Natural Sciences and Engineering Research Council of Canada (NSERC).

[1] E. Bauer, G. Hilscher, H. Michor, Ch. Paul, E. W. Scheidt, A. Griбанov, Yu. Seropegin, H. Noël, M. Sigrist, and P. Rogl, Heavy fermion superconductivity and magnetic order in non-centrosymmetric  $\text{CePt}_3\text{Si}$ , *Phys. Rev. Lett.* **92**, 027003 (2004).  
[2] M. Smidman, M. B. Salamon, H. Q. Yuan, and D. F. Agterberg, Superconductivity and spin-orbit coupling in non-centrosymmetric materials: A review, *Rep. Prog. Phys.* **80**, 036501 (2017).  
[3] L. P. Gor'kov and E. I. Rashba, Superconducting 2D system with lifted spin degeneracy: Mixed singlet-triplet state, *Phys. Rev. Lett.* **87**, 037004 (2001).  
[4] S. K. Ghosh, M. Smidman, T. Shang, J. F. Annett, A. D. Hillier, J. Quintanilla and H. Yuan, Recent progress on superconductors with time-reversal symmetry breaking, *J. Phys.: Condens. Matter* **33**, 033001 (2021).  
[5] A. B. Karki, Y. M. Xiong, I. Vekhter, D. Browne, P. W. Adams, D. P. Young, K. R. Thomas, Julia Y. Chan, H. Kim,

and R. Prozorov, Structure and physical properties of the non-centrosymmetric superconductor  $\text{Mo}_3\text{Al}_2\text{C}$ , *Phys. Rev. B* **82**, 064512 (2010).  
[6] J. K. Bao, J. Y. Liu, C. W. Ma, Z. H. Meng, Z. T. Tang, Y. L. Sun, H. F. Zhai, H. Jiang, H. Bai, C. M. Feng, Z. A. Xu, and G. H. Cao, Superconductivity in quasi-one-dimensional  $\text{K}_2\text{Cr}_3\text{As}_3$  with significant electron correlations, *Phys. Rev. X* **5**, 011013 (2015).  
[7] P. Fulde and R. A. Ferrell, Superconductivity in a strong spin-exchange field, *Phys. Rev.* **135**, A550 (1964).  
[8] A. I. Larkin and Y. N. Ovchinnikov, Nonuniform state of superconductors, *Zh. Eksp. Teor. Fiz.* **47**, 1136 (1964) [*Sov. Phys. JETP* **20**, 762 (1965)].  
[9] H. Takeya, M. ElMassalami, S. Kasahara, and K. Hirata, Specific-heat studies of the spin-orbit interaction in noncentrosymmetric  $\text{Li}_2(\text{Pd}_{1-x}\text{Pt}_x)_3\text{B}$  ( $x = 0, 0.5, 1$ ) superconductors, *Phys. Rev. B* **76**, 104506 (2007).

- [10] J. Chen, M. B. Salamon, S. Akutagawa, J. Akimitsu, J. Singleton, J. L. Zhang, L. Jiao, and H. Q. Yuan, Evidence of nodal gap structure in the noncentrosymmetric superconductor  $Y_2C_3$ , *Phys. Rev. B* **83**, 144529 (2011).
- [11] S. Kuroiwa, Y. Saura, J. Akimitsu, M. Hiraishi, M. Miyazaki, K. H. Satoh, S. Takeshita, and R. Kadono, Multigap Superconductivity in sesquicarbides  $La_2C_3$  and  $Y_2C_3$ , *Phys. Rev. Lett.* **100**, 097002 (2008).
- [12] J. Chen, L. Jiao, J. L. Zhang, Y. Chen, L. Yang, M. Nicklas, F. Steglich, and H. Q. Yuan, Evidence for two-gap superconductivity in the non-centrosymmetric compound  $LaNiC_2$ , *New J. Phys.* **15**, 053005 (2013).
- [13] M. Sato and Y. Ando, Topological superconductors: A review, *Rep. Prog. Phys.* **80**, 076501 (2017).
- [14] J. Garaud, A. Korneev, A. Samoilenka, A. Molochkov, E. Babaev, and M. Chernodub, Counterpart of the Chandrasekhar-Kendall state in noncentrosymmetric superconductors, *Phys. Rev. B* **108**, 014504 (2023).
- [15] D. Singh, J. A. T. Barker, T. Arumugam, A. D. Hillier, D. M. Paul, and R. P. Singh, Superconducting properties and  $\mu$ SR study of the noncentrosymmetric superconductor  $Nb_{0.5}Os_{0.5}$ , *J. Phys.: Condens. Matter* **30**, 075601 (2018).
- [16] D. Singh, Sajilesh K. P., Sourav Marik, P. K. Biswas, A. D. Hillier, and R. P. Singh, Nodeless  $s$ -wave superconductivity in the  $\alpha$ -Mn structure type noncentrosymmetric superconductor TaOs: A  $\mu$ SR study, *J. Phys.: Condens. Matter* **32**, 015602 (2020).
- [17] D. Singh, Sajilesh K. P., Sourav Marik, A. D. Hillier, and R. P. Singh, Superconducting and normal state properties of the noncentrosymmetric superconductor  $NbOs_2$  investigated by muon spin relaxation and rotation, *Phys. Rev. B* **99**, 014516 (2019).
- [18] D. Singh, A. D. Hillier, and R. P. Singh, Type-I superconductivity in the noncentrosymmetric superconductor BeAu, *Phys. Rev. B* **99**, 134509 (2019).
- [19] Sajilesh K. P., D. Singh, P. K. Biswas, Gavin B. G. Stenning, A. D. Hillier, and R. P. Singh, Investigations of the superconducting ground state of  $Zr_3Ir$ : Introducing a new noncentrosymmetric superconductor, *Phys. Rev. Mater.* **3**, 104802 (2019).
- [20] M. Mandal, C. Patra, A. Kataria, D. Singh, P. K. Biswas, J. S. Lord, A. D. Hillier, and R. P. Singh, Superconducting ground state of the nonsymmorphic superconducting compound  $Zr_2Ir$ , *Phys. Rev. B* **104**, 054509 (2021).
- [21] J. A. T. Barker, B. D. Breen, R. Hanson, A. D. Hillier, M. R. Lees, G. Balakrishnan, D. McK. Paul, and R. P. Singh, Superconducting and normal-state properties of the noncentrosymmetric superconductor  $Re_3Ta$ , *Phys. Rev. B* **98**, 104506 (2018).
- [22] P. K. Biswas, A. D. Hillier, M. R. Lees, and D. McK. Paul, Comparative study of the centrosymmetric and noncentrosymmetric superconducting phases of  $Re_3W$  using muon spin spectroscopy and heat capacity measurements, *Phys. Rev. B* **85**, 134505 (2012).
- [23] P. K. Biswas, M. R. Lees, A. D. Hillier, R. I. Smith, W. G. Marshall, and D. McK. Paul, Structure and superconductivity of two different phases of  $Re_3W$ , *Phys. Rev. B* **84**, 184529 (2011).
- [24] R. P. Singh, A. D. Hillier, B. Mazidian, J. Quintanilla, J. F. Annett, D. M. Paul, G. Balakrishnan, and M. R. Lees, Detection of time-reversal symmetry breaking in the noncentrosymmetric superconductor  $Re_6Zr$  using muon-spin spectroscopy, *Phys. Rev. Lett.* **112**, 107002 (2014).
- [25] D. Singh, J. A. T. Barker, A. Thamizhavel, D. McK. Paul, A. D. Hillier, and R. P. Singh, Time-reversal symmetry breaking in the noncentrosymmetric superconductor  $Re_6Hf$ : Further evidence for unconventional behavior in the  $\alpha$ -Mn family of materials, *Phys. Rev. B* **96**, 180501(R) (2017).
- [26] D. Singh, Sajilesh K. P., J. A. T. Barker, D. McK. Paul, A. D. Hillier, and R. P. Singh, Time-reversal symmetry breaking in the noncentrosymmetric superconductor  $Re_6Ti$ , *Phys. Rev. B* **97**, 100505(R) (2018).
- [27] S. Sharma, Arushi, K. Motla, J. Beare, M. Nugent, M. Pula, T. J. Munsie, A. D. Hillier, R. P. Singh, and G. M. Luke, Fully gapped superconductivity in centrosymmetric and noncentrosymmetric Re-B compounds probed with  $\mu$ SR, *Phys. Rev. B* **103**, 104507 (2021).
- [28] Arushi, D. Singh, P. K. Biswas, A. D. Hillier, and R. P. Singh, Unconventional superconducting properties of noncentrosymmetric  $Re_{5.5}Ta$ , *Phys. Rev. B* **101**, 144508 (2020).
- [29] T. Shang, M. Smidman, S. K. Ghosh, C. Baines, L. J. Chang, D. J. Gawryluk, J. A. T. Barker, R. P. Singh, D. McK. Paul, G. Balakrishnan, E. Pomjakushina, M. Shi, M. Medarde, A. D. Hillier, H. Q. Yuan, J. Quintanilla, J. Mesot, and T. Shiroka, Time-reversal symmetry breaking in Re-based superconductors, *Phys. Rev. Lett.* **121**, 257002 (2018).
- [30] A. B. Karki, Y. M. Xiong, N. Haldolaarachchige, S. Stadler, I. Vekhter, P. W. Adams, D. P. Young, W. A. Phelan, and J. Y. Chan, Physical properties of the noncentrosymmetric superconductor  $Nb_{0.18}Re_{0.82}$ , *Phys. Rev. B* **83**, 144525 (2011).
- [31] J. A. T. Barker, D. Singh, A. Thamizhavel, A. D. Hillier, M. R. Lees, G. Balakrishnan, D. McK. Paul, and R. P. Singh, Unconventional superconductivity in  $La_7Ir_3$  revealed by muon spin relaxation: Introducing a new family of noncentrosymmetric superconductor that breaks time-reversal symmetry, *Phys. Rev. Lett.* **115**, 267001 (2015).
- [32] D. Singh, M. S. Scheurer, A. D. Hillier, D. T. Adroja, and R. P. Singh, Time-reversal-symmetry breaking and unconventional pairing in the noncentrosymmetric superconductor  $La_7Rh_3$ , *Phys. Rev. B* **102**, 134511 (2020).
- [33] Arushi, D. Singh, A. D. Hillier, M. S. Scheurer, and R. P. Singh, Time-reversal symmetry breaking and multigap superconductivity in the noncentrosymmetric superconductor  $La_7Ni_3$ , *Phys. Rev. B* **103**, 174502 (2021).
- [34] K. P. Sajilesh, K. Motla, P. K. Meena, A. Kataria, C. Patra, Somesh K., A. D. Hillier, and R. P. Singh, Superconductivity in noncentrosymmetric  $NbReSi$  investigated by muon spin rotation and relaxation, *Phys. Rev. B* **105**, 094523 (2022).
- [35] T. Shang, D. J. Gawryluk, J. A. T. Verezhak, E. Pomjakushina, M. Shi, M. Medarde, J. Mesot, and T. Shiroka, Structure and superconductivity in the binary  $Re_{1-x}Mo_x$  alloys, *Phys. Rev. Mater.* **3**, 024801 (2019).
- [36] T. Shang, C. Baines, L. J. Chang, D. J. Gawryluk, E. Pomjakushina, M. Shi, M. Medarde, and T. Shiroka,  $Re_{1-x}Mo_x$  as an ideal test case of time-reversal symmetry breaking in unconventional superconductors, *npj Quant. Mater.* **5**, 76 (2020).
- [37] S. Sharma, Sajilesh K. P., A. D. S. Richards, J. Gautreau, M. Pula, J. Beare, K. M. Kojima, S. Yoon, Y. Cai, R. K. Kushwaha, T. Agarwal, E. S. Sørensen, R. P. Singh, and G. M. Luke, Evidence for nonunitary triplet-pairing superconductivity in



- noncentrosymmetric TaRuSi and comparison with isostructural TaReSi, *Phys. Rev. B* **108**, 144510 (2023).
- [38] J. Quintanilla, A. D. Hillier, J. F. Annett, and R. Cywinski, Relativistic analysis of the pairing symmetry of the noncentrosymmetric superconductor LaNiC<sub>2</sub>, *Phys. Rev. B* **82**, 174511 (2010).
- [39] S. L. Lee, S. H. Kilcoyne, and R. Cywinski, *MuonScience: Muons in Physics, Chemistry, and Materials* (Taylor & Francis, Abingdon, 1999).
- [40] J. Bardeen, L. N. Cooper, and J. R. Schrieffer, Theory of superconductivity, *Phys. Rev.* **108**, 1175 (1957).
- [41] G. Morris and R. Heffner, A method of achieving accurate zero-field conditions using muonium, *Phys. B: Condens. Matter* **326**, 252 (2003).
- [42] A. Suter and B. M. Wojek, Musrfit: A free platform-independent framework for  $\mu$ SR data analysis, *Phys. Proc.* **30**, 69 (2012).
- [43] J. Rodríguez-Carvajal, Recent advances in magnetic structure determination by neutron powder diffraction, *Phys. B: Condens. Matter* **192**, 55 (1993).
- [44] E. Helfand and N. R. Werthamer, Temperature and purity dependence of the superconducting critical field, H<sub>c2</sub>. II, *Phys. Rev.* **147**, 288 (1966).
- [45] N. R. Werthamer, E. Helfand, and P. C. Hohenberg, Temperature and purity dependence of the superconducting critical field, H<sub>c2</sub>. III. Electron spin and spin-orbit effects, *Phys. Rev.* **147**, 295 (1966).
- [46] M. Tinkham, *Introduction to Superconductivity*, 2nd ed. (McGraw-Hill, New York, 1996).
- [47] T. Klimczuk, F. Ronning, V. Sidorov, R. J. Cava, and J. D. Thompson, Physical properties of the noncentrosymmetric superconductor Mg<sub>10</sub>Ir<sub>19</sub>B<sub>16</sub>, *Phys. Rev. Lett.* **99**, 257004 (2007).
- [48] A. E. Koshelev, K. Willa, R. Willa, M. P. Smylie, J.-K. Bao, D. Y. Chung, M. G. Kanatzidis, W.-K. Kwok, and U. Welp, Melting of vortex lattice in the magnetic superconductor RbEuFe<sub>4</sub>As<sub>4</sub>, *Phys. Rev. B* **100**, 094518 (2019).
- [49] G. Blatter, M. V. Feigel'man, V. B. Geshkenbein, A. I. Larkin, and V. M. Vinokur, Vortices in high-temperature superconductors, *Rev. Mod. Phys.* **66**, 1125 (1994).
- [50] O. Prakash, A. Thamizhavel, and S. Ramakrishnan, Multiband superconductivity in Lu<sub>3</sub>Os<sub>4</sub>Ge<sub>13</sub>, *Supercond. Sci. Technol.* **28**, 115012 (2015).
- [51] W. L. McMillan, Transition temperature of strong-coupled superconductors, *Phys. Rev.* **167**, 331 (1968).
- [52] A. Bhattacharyya, D. Adroja, N. Kase, A. Hillier, J. Akimitsu, and A. Strydom, Unconventional superconductivity in Y<sub>5</sub>Rh<sub>6</sub>Sn<sub>18</sub> probed by muon spin relaxation, *Sci. Rep.* **5**, 12926 (2015).
- [53] D. T. Adroja, A. Bhattacharyya, M. Telling, Yu. Feng, M. Smidman, B. Pan, J. Zhao, A. D. Hillier, F. L. Pratt, and A. M. Strydom, Superconducting ground state of quasi-one-dimensional K<sub>2</sub>Cr<sub>3</sub>As<sub>3</sub> investigated using  $\mu$ SR measurements, *Phys. Rev. B* **92**, 134505 (2015).
- [54] C. Caroli, P. G. de Gennes, and J. Matricon, Bound Fermion states on a vortex line in a type II superconductor, *Phys. Lett.* **9**, 307 (1964).
- [55] C. Patra, T. Agarwal, Rajeshwari R. Chaudhari, and R. P. Singh, Two-dimensional multigap superconductivity in bulk 2H-TaSeS, *Phys. Rev. B* **106**, 134515 (2022).
- [56] A. A. Abrikosov, On the magnetic properties of superconductors of the second group, *J. Exp. Theor. Phys. (USSR)* **32**, 1442 (1957).
- [57] G. Aeppli, E. J. Ansaldo, J. H. Brewer, R. J. Cava, R. F. Kiefl, S. R. Kreitzman, G. M. Luke, and D. R. Noakes, Magnetic penetration depth and flux-pinning effects in high-Tc superconductor La<sub>1.85</sub>Sr<sub>0.15</sub>CuO, *Phys. Rev. B* **35**, 7129 (1987).
- [58] E. H. Brandt, Properties of the ideal Ginzburg-Landau vortex lattice, *Phys. Rev. B* **68**, 054506 (2003).
- [59] A. Carrington and F. Manzano, Magnetic penetration depth of MgB<sub>2</sub>, *Physica C: Superconduct.* **385**, 205 (2003).
- [60] R. S. Hayano, Y. J. Uemura, J. Imazato, N. Nishida, T. Yamazaki, and R. Kubo, Zero- and low-field spin relaxation studied by positive muons, *Phys. Rev. B* **20**, 850 (1979).
- [61] A. D. Hillier, J. Quintanilla, and R. Cywinski, Evidence for time-reversal symmetry breaking in the noncentrosymmetric superconductor LaNiC<sub>2</sub>, *Phys. Rev. Lett.* **102**, 117007 (2009).
- [62] D. Adroja, A. Bhattacharyya, M. Smidman, A. Hillier, Y. Feng, B. Pan, J. Zhao, M. R. Lees, A. Strydom, and P. K. Biswas, Nodal superconducting gap structure in the quasi-one-dimensional Cs<sub>2</sub>Cr<sub>3</sub>As<sub>3</sub> investigated using  $\mu$ SR measurements, *J. Phys. Soc. Jpn.* **86**, 044710 (2017).
- [63] J. A. T. Barker, R. P. Singh, A. D. Hillier, and D. McK. Paul, Probing the superconducting ground state of the rare-earth ternary boride superconductors RRuB<sub>2</sub> (R = Lu, Y) using muon-spin rotation and relaxation, *Phys. Rev. B* **97**, 094506 (2018).
- [64] A. D. Hillier and R. Cywinski, The classification of superconductors using muon spin rotation, *Appl. Magn. Reson.* **13**, 95 (1997).
- [65] M. Mandal, A. Kataria, C. Patra, D. Singh, P. K. Biswas, A. D. Hillier, T. Das, and R. P. Singh, Time-reversal symmetry breaking in frustrated superconductor Re<sub>2</sub>Hf, *Phys. Rev. B* **105**, 094513 (2022).
- [66] Y. J. Uemura, L. P. Le, G. M. Luke, B. J. Sternlieb, W. D. Wu, J. H. Brewer, T. M. Riseman, C. L. Seaman, M. Maple, M. Ishikawa, D. G. Hinks, J. D. Jorgensen, G. Saito, and H. Yamochi, Basic similarities among cuprate, bismuthate, organic, Chevrel-phase, and heavy-fermion superconductors shown by penetration-depth measurements, *Phys. Rev. Lett.* **66**, 2665 (1991).